

An adaptive hp -refinement strategy with computable guaranteed bound on the error reduction factor[☆]

Patrik Daniel^{a,b,*}, Alexandre Ern^{b,a}, Iain Smears^c, Martin Vohralík^{a,b}

^a*Inria, 2 rue Simone Iff, 75589 Paris, France*

^b*Université Paris-Est, CERMICS (ENPC), 77455 Marne-la-Vallée 2, France*

^c*Department of Mathematics, University College London, Gower Street, WC1E 6BT London, United Kingdom*

Abstract

We propose a new practical adaptive refinement strategy for hp -finite element approximations of elliptic problems. Following recent theoretical developments in polynomial-degree-robust a posteriori error analysis, we solve two types of discrete local problems on vertex-based patches. The first type involves the solution on each patch of a mixed finite element problem with homogeneous Neumann boundary conditions, which leads to an $\mathbf{H}(\operatorname{div}, \Omega)$ -conforming equilibrated flux. This, in turn, yields a guaranteed upper bound on the error and serves to mark mesh vertices for refinement via Dörfler’s bulk-chasing criterion. The second type of local problems involves the solution, on patches associated with marked vertices only, of two separate primal finite element problems with homogeneous Dirichlet boundary conditions, which serve to decide between h -, p -, or hp -refinement. Altogether, we show that these ingredients lead to a computable guaranteed bound on the ratio of the errors between successive refinements (error reduction factor). In a series of numerical experiments featuring smooth and singular solutions, we study the performance of the proposed hp -adaptive strategy and observe exponential convergence rates. We also investigate the

[☆]This project has received funding from the European Research Council (ERC) under the European Union’s Horizon 2020 research and innovation program (grant agreement No 647134 GATIPOR).

*Corresponding author

Email addresses: patrik.daniel@inria.fr (Patrik Daniel), alexandre.ern@enpc.fr (Alexandre Ern), i.smears@ucl.ac.uk (Iain Smears), martin.vohralik@inria.fr (Martin Vohralík)

accuracy of our bound on the reduction factor by evaluating the ratio of the predicted reduction factor relative to the true error reduction, and we find that this ratio is in general quite close to the optimal value of one.

Keywords: a posteriori error estimate, hp -refinement, finite element method, error reduction, equilibrated flux, residual lifting

2010 MSC: 65N30, 65N15, 65N50

1. Introduction

Adaptive discretization methods constitute an important tool in computational science and engineering. Since the pioneering works on the hp -finite element method by Gui and Babuška [21, 22] and Babuška and Guo [1, 2] in the 1980s, where it was shown that for one-dimensional problems hp -refinement leads to exponential convergence with respect to the number of degrees of freedom on *a priori* adapted meshes, there has been a great amount of work devoted to developing *adaptive hp -refinement* strategies based on *a posteriori error estimates*. Convergence of hp -adaptive finite element approximations for elliptic problems, has, though, been addressed only very recently in Dörfler and Heuveline [17], Bürg and Dörfler [7], and Bank, Parsania, and Sauter [3]. The first optimality result we are aware of is by Canuto *et al.* [8], where an important ingredient is the hp -coarsening routine by Binev [4, 5]. These works extend to the hp -context the previous h -convergence and optimality results by Dörfler [16], Morin, Nochetto, and Siebert [27, 28], Stevenson [31], Cascón *et al.* [11], Carstensen *et al.* [10], see also Nochetto *et al.* [29] and the references therein. It is worth mentioning that most of the available convergence results are formulated for adaptive methods driven by residual-type a posteriori error estimators; other estimators have in particular been addressed in Cascón and Nochetto [12] and Kreuzer and Siebert [24].

A key ingredient for adaptive hp -refinement is a local criterion in each mesh cell marked for refinement that allows one to decide whether h -, p -, or hp -refinement should be performed. There is a substantial amount of such criteria

proposed in the literature; a computational overview can be found in Mitchell
 25 and McClain [26, 25]. Some of the mathematically motivated hp -decision criteria
 include, among others, those proposed by Eibner and Melenk [18], Houston and
 Süli [23] which both estimate the local regularity of the exact weak solution.
 Our proposed strategy fits into the group of algorithms based on solving local
 boundary value problems allowing us to forecast the benefits of performing h -
 30 or p -refinement, as recently considered in, e.g., [7, 17]. Similarly to [17], we use
 the *local* finite element spaces associated with a specific type of refinement to
 perform the above forecast and to take the local hp -refinement decision. We also
 mention the work of Demkowicz *et al.* [13] for an earlier, yet more expensive,
 version of the look-ahead idea, where it is proposed to solve an auxiliary problem
 35 on a *global* finite element space corresponding to a mesh refined uniformly either
 in h or in p .

In the present work, we focus on the Poisson model problem with (homoge-
 neous) Dirichlet boundary conditions. In weak form, the model problem reads
 as follows: Find $u \in H_0^1(\Omega)$ such that

$$(\nabla u, \nabla v) = (f, v) \quad \forall v \in H_0^1(\Omega), \quad (1.1)$$

where $\Omega \subset \mathbb{R}^d$, $d = 2, 3$, is a polygonal/polyhedral domain (open, bounded,
 and connected set) with a Lipschitz boundary, $f \in L^2(\Omega)$, $H_0^1(\Omega)$ denotes
 the Sobolev space of all functions in $L^2(\Omega)$ which have all their first-order
 weak derivatives in $L^2(\Omega)$ and a zero trace on $\partial\Omega$, and (\cdot, \cdot) stands for the
 $L^2(\Omega)$ or $[L^2(\Omega)]^d$ inner product. Our first goal is to propose a reliable and
 computationally-efficient *hp-adaptive strategy* to approximate the model prob-
 lem (1.1) that hinges on the recent theoretical developments on polynomial-
 degree-robust a posteriori error estimates due to Braess *et al.* [6] and Ern and
 Vohralík [19, 20]. The present hp -adaptive algorithm follows the well-established
 paradigm based on an iterative loop where each step consists of the following
 four modules:

$$\text{SOLVE} \rightarrow \text{ESTIMATE} \rightarrow \text{MARK} \rightarrow \text{REFINE}. \quad (1.2)$$

Here, SOLVE stands for application of the conforming finite element method on a matching (no hanging nodes) simplicial mesh to approximate the model problem (1.1); spatially-varying polynomial degree is allowed. The module ESTIMATE is based on an equilibrated flux a posteriori error estimate, obtained by solving, for each mesh vertex, a local mixed finite element problem with a (homogeneous) Neumann boundary condition on the patch of cells sharing the given vertex. The module MARK is based on a bulk-chasing criterion inspired by the well-known Dörfler’s marking [16]; here we mark mesh vertices and not simplices since we observe a smoother performance in practice and since we later work with some vertex-based auxiliary quantities.

The module REFINE, where we include our hp -decision criterion, is organized into three steps. First, we solve two local finite element problems on each patch of simplices attached to a mesh vertex marked for refinement, with either the mesh refined or the polynomial degree increased. This is inspired by the key observation from [19, Lemma 3.23] that guaranteed local efficiency can be materialized by some local conforming finite element solves. These conforming residual liftings allow us, in particular, to estimate the effect of applying h - or p -refinement, and lead to a partition of the set of marked vertices into two disjoint subsets, one collecting the mesh vertices flagged for h -refinement and the other collecting the mesh vertices flagged for p -refinement. The second step of the module REFINE uses these two subsets to flag the simplices for h -, p -, or hp -refinement. Finally, the third step of the module REFINE uses the above sets of flagged simplices to build the next simplicial mesh and the next polynomial-degree distribution. Let us mention that recently, Dolejší *et al.* [15] also devised an hp -adaptive algorithm driven by polynomial-degree-robust a posteriori error estimates based on the equilibrated fluxes from [6, 19, 20]. The differences with the present work are that the interior penalty discontinuous Galerkin method is considered in [15], and more importantly, that the present hp -decision criterion hinges on local primal solves on patches around marked vertices.

The second goal of the present work is to show that the proposed hp -adaptive strategy automatically leads to a *computable guaranteed bound* on the error

reduction factor between two consecutive steps of the adaptive loop (1.2). More precisely, we show how to compute explicitly a real number $C_{\text{red}} \in [0, 1]$ so that

$$\|\nabla(u - u_{\ell+1})\| \leq C_{\text{red}} \|\nabla(u - u_{\ell})\|, \quad (1.3)$$

where u_{ℓ} denotes the discrete solution on ℓ -th iteration of the adaptive loop, see Theorem 5.2 below. Thus the number C_{red} gives a guaranteed (constant-free) bound on the ratio of the errors between successive refinements. This must not be confused with saying that the error is guaranteed to be reduced, since the case $C_{\text{red}} = 1$ cannot be ruled out in general without additional assumptions (e.g. an interior node property, see [27] for further details). The computation of C_{red} crucially relies on a combined use of the equilibrated fluxes and of the conforming residual liftings, which were already used for the error estimation and hp -refinement decision criterion respectively. It is worth noting that we consider a homogeneous Dirichlet boundary condition for the local residual liftings in order to obtain an estimate on the error reduction factor that is as sharp as possible.

The rest of this manuscript is organized as follows. Section 2 describes the discrete setting and introduces some useful notation. Section 3 presents the modules SOLVE, ESTIMATE, and MARK, whereas Section 4 presents the module REFINE. Section 5 contains our main result on a guaranteed bound on the error reduction factor. Finally, numerical experiments on two-dimensional test cases featuring smooth and singular solutions are discussed in Section 6, and conclusions are drawn in Section 7.

2. Discrete setting

The main purpose of the adaptive loop (1.2) is to generate a sequence of finite-dimensional H_0^1 -conforming finite element spaces $(V_{\ell})_{\ell \geq 0}$, where the integer $\ell \geq 0$ stands for the iteration counter in (1.2). H_0^1 -conformity means that $V_{\ell} \subset H_0^1(\Omega)$ for all $\ell \geq 0$. In this work, we shall make the following nestedness assumption:

$$V_{\ell} \subset V_{\ell+1}, \quad \forall \ell \geq 0. \quad (2.1)$$

The space V_ℓ is built from two ingredients: (i) a matching simplicial mesh \mathcal{T}_ℓ of the computational domain Ω , that is, a finite collection of (closed) non-overlapping simplices $K \in \mathcal{T}_\ell$ covering $\bar{\Omega}$ exactly and such that the intersection of two different simplices is either empty, a common vertex, a common edge, or a common face; (ii) a polynomial-degree distribution described by the vector $\mathbf{p}_\ell := (p_{\ell,K})_{K \in \mathcal{T}_\ell}$ that assigns a polynomial degree to each simplex $K \in \mathcal{T}_\ell$. The conforming finite element space V_ℓ is then defined as

$$V_\ell := \mathbb{P}_{\mathbf{p}_\ell}(\mathcal{T}_\ell) \cap H_0^1(\Omega), \quad \forall \ell \geq 0,$$

where $\mathbb{P}_{\mathbf{p}_\ell}(\mathcal{T}_\ell)$ denotes the space of piecewise polynomials of total degree $p_{\ell,K} \geq 1$ on each simplex $K \in \mathcal{T}_\ell$. In other words, any function $v_\ell \in V_\ell$ satisfies $v_\ell \in H_0^1(\Omega)$ and $v_\ell|_K \in \mathbb{P}_{p_{\ell,K}}(K)$ for all $K \in \mathcal{T}_\ell$, where for an integer $p \geq 1$, $\mathbb{P}_p(K)$ stands for the space of polynomials of total degree at most p on the
90 simplex K .

The initial mesh \mathcal{T}_0 and the initial polynomial-degree distribution \mathbf{p}_0 are given, and the purpose of each step $\ell \geq 0$ of the adaptive loop (1.2) is to produce the next mesh $\mathcal{T}_{\ell+1}$ and the next polynomial-degree distribution $\mathbf{p}_{\ell+1}$. In order to ensure the nestedness property (2.1), the following two properties
95 are to be satisfied: (i) The sequence $(\mathcal{T}_\ell)_{\ell \geq 0}$ is hierarchical, i.e., for all $\ell \geq 0$ and all $\tilde{K} \in \mathcal{T}_{\ell+1}$, there is a unique simplex $K \in \mathcal{T}_\ell$, called the parent of \tilde{K} so that $\tilde{K} \subseteq K$; (ii) The local polynomial degree is locally increasing, i.e., for all $\ell \geq 0$ and all $\tilde{K} \in \mathcal{T}_{\ell+1}$, $p_{\ell+1,\tilde{K}} \geq p_{\ell,K}$ where $K \in \mathcal{T}_\ell$ is the parent of \tilde{K} . Moreover, we assume the following shape-regularity property: There exists a constant $\kappa_{\mathcal{T}} > 0$
100 such that $\max_{K \in \mathcal{T}_\ell} h_K / \rho_K \leq \kappa_{\mathcal{T}}$ for all $\ell \geq 0$, where h_K is the diameter of K and ρ_K is the diameter of the largest ball inscribed in K .

Before closing this section, we introduce some further useful notation. The set of vertices \mathcal{V}_ℓ of each mesh \mathcal{T}_ℓ is decomposed into $\mathcal{V}_\ell^{\text{int}}$ and $\mathcal{V}_\ell^{\text{ext}}$, the set of inner and boundary vertices, respectively. For each vertex $\mathbf{a} \in \mathcal{V}_\ell$, the so-called
105 hat function $\psi_\ell^{\mathbf{a}}$ is the continuous, piecewise affine function that takes the value 1 at the vertex \mathbf{a} and the value 0 at all the other vertices of \mathcal{V}_ℓ ; the function $\psi_\ell^{\mathbf{a}}$ is in V_ℓ for all $\mathbf{a} \in \mathcal{V}_\ell^{\text{int}}$. Moreover, we consider the simplex patch $\mathcal{T}_\ell^{\mathbf{a}} \subset \mathcal{T}_\ell$ which

is the collection of the simplices in \mathcal{T}_ℓ sharing the vertex $\mathbf{a} \in \mathcal{V}_\ell$, and we denote by $\omega_\ell^{\mathbf{a}}$ the corresponding open subdomain. Finally, for each simplex $K \in \mathcal{T}_\ell$, \mathcal{V}_K denotes the set of vertices of K .

3. The modules SOLVE, ESTIMATE, and MARK

In this section we present the modules SOLVE, ESTIMATE, and MARK from the adaptive loop (1.2). Let $\ell \geq 0$ denote the current iteration number.

3.1. The module SOLVE

The module SOLVE takes as input the H_0^1 -conforming finite element space V_ℓ and outputs the discrete function $u_\ell \in V_\ell$ which is the unique solution of

$$(\nabla u_\ell, \nabla v_\ell) = (f, v_\ell) \quad \forall v_\ell \in V_\ell. \quad (3.1)$$

3.2. The module ESTIMATE

Following [14, 6, 19, 15, 20], see also the references therein, the module ESTIMATE relies on an equilibrated flux a posteriori error estimate on the energy error $\|\nabla(u - u_\ell)\|$. The module ESTIMATE takes as input the finite element solution u_ℓ and outputs a collection of local error indicators $\{\eta_K\}_{K \in \mathcal{T}_\ell}$. The equilibrated flux is constructed locally from mixed finite element solves on the simplex patches $\mathcal{T}_\ell^{\mathbf{a}}$ attached to each vertex $\mathbf{a} \in \mathcal{V}_\ell$. For this construction, we consider as in [15] the local polynomial degree $p_{\mathbf{a}}^{\text{est}} := \max_{K \in \mathcal{T}_\ell^{\mathbf{a}}} p_{\ell, K}$ (any other choice so that $p_{\mathbf{a}}^{\text{est}} \geq \max_{K \in \mathcal{T}_\ell^{\mathbf{a}}} p_{\ell, K}$ can also be employed). We consider the local Raviart–Thomas–Nédélec mixed finite element spaces $(\mathbf{V}_\ell^{\mathbf{a}}, Q_\ell^{\mathbf{a}})$ which are defined for all $\mathbf{a} \in \mathcal{V}_\ell^{\text{int}}$ by

$$\mathbf{V}_\ell^{\mathbf{a}} := \{\mathbf{v}_\ell \in \mathbf{H}(\text{div}, \omega_\ell^{\mathbf{a}}); \mathbf{v}_\ell|_K \in \mathbf{RTN}_{p_{\mathbf{a}}^{\text{est}}}(K), \forall K \in \mathcal{T}_\ell^{\mathbf{a}}, \mathbf{v}_\ell \cdot \mathbf{n}_{\omega_\ell^{\mathbf{a}}} = 0 \text{ on } \partial\omega_\ell^{\mathbf{a}}\},$$

$$Q_\ell^{\mathbf{a}} := \{q_\ell \in \mathbb{P}_{p_{\mathbf{a}}^{\text{est}}}(\mathcal{T}_\ell^{\mathbf{a}}); (q_\ell, 1)_{\omega_\ell^{\mathbf{a}}} = 0\},$$

and, for all $\mathbf{a} \in \mathcal{V}_\ell^{\text{ext}}$,

$$\mathbf{V}_\ell^{\mathbf{a}} := \{\mathbf{v}_\ell \in \mathbf{H}(\text{div}, \omega_\ell^{\mathbf{a}}); \mathbf{v}_\ell|_K \in \mathbf{RTN}_{p_{\mathbf{a}}^{\text{est}}}(K), \forall K \in \mathcal{T}_\ell^{\mathbf{a}}, \mathbf{v}_\ell \cdot \mathbf{n}_{\omega_\ell^{\mathbf{a}}} = 0 \text{ on } \partial\omega_\ell^{\mathbf{a}} \setminus \partial\Omega\},$$

$$Q_\ell^{\mathbf{a}} := \mathbb{P}_{p_{\mathbf{a}}^{\text{est}}}(\mathcal{T}_\ell^{\mathbf{a}}),$$

where $\mathbf{RTN}_{p_{\mathbf{a}}^{\text{est}}}(K) := [\mathbb{P}_{p_{\mathbf{a}}^{\text{est}}}(K)]^d + \mathbb{P}_{p_{\mathbf{a}}^{\text{est}}}(K)\mathbf{x}$, and $\mathbf{n}_{\omega_{\ell}^{\mathbf{a}}}$ denotes the unit outward-pointing normal to $\omega_{\ell}^{\mathbf{a}}$.

Definition 3.1 (Flux reconstruction $\boldsymbol{\sigma}_{\ell}$). *Let u_{ℓ} solve (3.1). The global equilibrated flux $\boldsymbol{\sigma}_{\ell}$ is constructed as $\boldsymbol{\sigma}_{\ell} := \sum_{\mathbf{a} \in \mathcal{V}_{\ell}} \boldsymbol{\sigma}_{\ell}^{\mathbf{a}}$, where, for each vertex $\mathbf{a} \in \mathcal{V}_{\ell}$, $(\boldsymbol{\sigma}_{\ell}^{\mathbf{a}}, \gamma_{\ell}^{\mathbf{a}}) \in \mathbf{V}_{\ell}^{\mathbf{a}} \times Q_{\ell}^{\mathbf{a}}$ solves*

$$\begin{aligned} (\boldsymbol{\sigma}_{\ell}^{\mathbf{a}}, \mathbf{v}_{\ell})_{\omega_{\ell}^{\mathbf{a}}} - (\gamma_{\ell}^{\mathbf{a}}, \nabla \cdot \mathbf{v}_{\ell})_{\omega_{\ell}^{\mathbf{a}}} &= -(\psi_{\ell}^{\mathbf{a}} \nabla u_{\ell}, \mathbf{v}_{\ell})_{\omega_{\ell}^{\mathbf{a}}} & \forall \mathbf{v}_{\ell} \in \mathbf{V}_{\ell}^{\mathbf{a}}, \\ (\nabla \cdot \boldsymbol{\sigma}_{\ell}^{\mathbf{a}}, q_{\ell})_{\omega_{\ell}^{\mathbf{a}}} &= (f \psi_{\ell}^{\mathbf{a}} - \nabla u_{\ell} \cdot \nabla \psi_{\ell}^{\mathbf{a}}, q_{\ell})_{\omega_{\ell}^{\mathbf{a}}} & \forall q_{\ell} \in Q_{\ell}^{\mathbf{a}}, \end{aligned}$$

or, equivalently,

$$\boldsymbol{\sigma}_{\ell}^{\mathbf{a}} := \arg \min_{\substack{\mathbf{v}_{\ell} \in \mathbf{V}_{\ell}^{\mathbf{a}}, \\ \nabla \cdot \mathbf{v}_{\ell} = \Pi_{Q_{\ell}^{\mathbf{a}}}(f \psi_{\ell}^{\mathbf{a}} - \nabla u_{\ell} \cdot \nabla \psi_{\ell}^{\mathbf{a}})}} \|\psi_{\ell}^{\mathbf{a}} \nabla u_{\ell} + \mathbf{v}_{\ell}\|_{\omega_{\ell}^{\mathbf{a}}},$$

and where $\boldsymbol{\sigma}_{\ell}^{\mathbf{a}}$ is extended by zero outside $\omega_{\ell}^{\mathbf{a}}$.

Note that the Neumann compatibility condition for the problem (3.2) is satisfied for all $\mathbf{a} \in \mathcal{V}_{\ell}^{\text{int}}$ (take $v_{\ell} = \psi_{\ell}^{\mathbf{a}}$ as a test function in (3.1)). Moreover, Definition 3.1 yields a globally $\mathbf{H}(\text{div}, \Omega)$ -conforming flux reconstruction $\boldsymbol{\sigma}_{\ell}$ such that, for all $K \in \mathcal{T}_{\ell}$, $(\nabla \cdot \boldsymbol{\sigma}_{\ell}, v_{\ell})_K = (f, v_{\ell})_K$ for all $v_{\ell} \in \mathbb{P}_{\min_{\mathbf{a} \in \mathcal{V}_K} p_{\mathbf{a}}^{\text{est}}}(K)$, see [15, Lemma 3.6]. Using the current notation, [15, Theorem 3.3] states the following result.

Theorem 3.2 (Guaranteed upper bound on the error). *Let u solve (1.1) and u_{ℓ} solve (3.1). Let $\boldsymbol{\sigma}_{\ell}$ be the equilibrated flux reconstruction of Definition 3.1. Then*

$$\|\nabla(u - u_{\ell})\| \leq \eta(\mathcal{T}_{\ell}) := \left\{ \sum_{K \in \mathcal{T}_{\ell}} \eta_K^2 \right\}^{\frac{1}{2}}, \quad \eta_K := \|\nabla u_{\ell} + \boldsymbol{\sigma}_{\ell}\|_K + \frac{h_K}{\pi} \|f - \nabla \cdot \boldsymbol{\sigma}_{\ell}\|_K. \quad (3.3)$$

As discussed in, e.g., [19, Remark 3.6], the term $\frac{h_K}{\pi} \|f - \nabla \cdot \boldsymbol{\sigma}_{\ell}\|_K$ represents, for all $K \in \mathcal{T}_{\ell}$, a local oscillation in the source datum f that, under suitable smoothness assumptions, converges to zero two orders faster than the error. To cover the whole computational range in our numerical experiments, this term is kept in the error indicator η_K .

130 *3.3. The module MARK*

The module MARK takes as input the local error estimators $\{\eta_K\}_{K \in \mathcal{T}_\ell}$ from Theorem 3.2 and outputs a set of marked vertices $\tilde{\mathcal{V}}_\ell^\theta \subset \mathcal{V}_\ell$ using a bulk-chasing criterion inspired by the well-known Dörfler’s marking criterion [16]. The reason why we mark vertices and not simplices is that our hp -decision criterion in the module REFINER (see Section 4 below) hinges on the solution of local primal solves posed on the patches $\mathcal{T}_\ell^{\mathbf{a}}$ associated with the marked vertices $\mathbf{a} \in \tilde{\mathcal{V}}_\ell^\theta$; we also observe in practice a smoother performance of the overall hp -adaptive procedure when marking vertices than when marking elements. Vertex-marking strategies are also considered, among others, in [27, 9].

For a subset $\mathcal{S} \subset \mathcal{T}_\ell$, we use the notation $\eta(\mathcal{S}) := \{\sum_{K \in \mathcal{S}} \eta_K^2\}^{1/2}$. In the module MARK, the set of marked vertices $\tilde{\mathcal{V}}_\ell^\theta$ is selected in such a way that

$$\eta\left(\bigcup_{\mathbf{a} \in \tilde{\mathcal{V}}_\ell^\theta} \mathcal{T}_\ell^{\mathbf{a}}\right) \geq \theta \eta(\mathcal{T}_\ell), \quad (3.4)$$

where $\theta \in (0, 1]$ is a fixed threshold. Letting

$$\mathcal{M}_\ell^\theta := \bigcup_{\mathbf{a} \in \tilde{\mathcal{V}}_\ell^\theta} \mathcal{T}_\ell^{\mathbf{a}} \subset \mathcal{T}_\ell \quad (3.5)$$

140 be the collection of all the simplices that belong to a patch associated with a marked vertex, we observe that (3.4) means that $\eta(\mathcal{M}_\ell^\theta) \geq \theta \eta(\mathcal{T}_\ell)$. To select a set $\tilde{\mathcal{V}}_\ell^\theta$ of minimal cardinality, the mesh vertices in \mathcal{V}_ℓ are sorted by comparing the vertex-based error estimators $\eta(\mathcal{T}_\ell^{\mathbf{a}})$ for all $\mathbf{a} \in \mathcal{V}_\ell$, and a greedy algorithm is employed to build the set $\tilde{\mathcal{V}}_\ell^\theta$. The module MARK is summarized in Algorithm 1.
 145 A possibly slightly larger set $\tilde{\mathcal{V}}_\ell^\theta$ can be constructed with linear cost in terms of the number of mesh vertices by using the algorithm proposed in [16, Section 5.2].

Algorithm 1 (module MARK)

```
1: procedure MARK( $\{\eta_K\}_{K \in \mathcal{T}_\ell}, \theta$ )
2:    $\triangleright$  Input: error indicators  $\{\eta_K\}_{K \in \mathcal{T}_\ell}$ , marking parameter  $\theta \in (0, 1]$ 
3:    $\triangleright$  Output: set of marked vertices  $\tilde{\mathcal{V}}_\ell^\theta$ 
4:   for all  $\mathbf{a} \in \mathcal{V}_\ell$  do
5:     Compute the vertex-based error estimator  $\eta(\mathcal{T}_\ell^{\mathbf{a}})$ 
6:   end for
7:   Sort the vertices according to  $\eta(\mathcal{T}_\ell^{\mathbf{a}})$ 
8:   Set  $\tilde{\mathcal{V}}_\ell^\theta := \emptyset$ 
9:   while  $\eta(\bigcup_{\mathbf{a} \in \tilde{\mathcal{V}}_\ell^\theta} \mathcal{T}_\ell^{\mathbf{a}}) < \theta \eta(\mathcal{T}_\ell)$  do
10:    Add to  $\tilde{\mathcal{V}}_\ell^\theta$  the next sorted vertex  $\mathbf{a} \in \mathcal{V}_\ell \setminus \tilde{\mathcal{V}}_\ell^\theta$ 
11:  end while
12: end procedure
```

4. The module REFINE

The module REFINE takes as input the set of marked vertices $\tilde{\mathcal{V}}_\ell^\theta$ and outputs the mesh $\mathcal{T}_{\ell+1}$ and the polynomial-degree distribution $\mathbf{p}_{\ell+1}$ to be used at the next step of the adaptive loop (1.2); the integer $\ell \geq 0$ is the current iteration number therein. This module is organized into three steps. First, an hp -decision is made on all the marked vertices so that each marked vertex $\mathbf{a} \in \tilde{\mathcal{V}}_\ell^\theta$ is flagged either for h -refinement or for p -refinement. This means that the set $\tilde{\mathcal{V}}_\ell^\theta$ is split into two disjoint subsets $\tilde{\mathcal{V}}_\ell^\theta = \tilde{\mathcal{V}}_\ell^h \cup \tilde{\mathcal{V}}_\ell^p$ with obvious notation (here we drop the superscript θ to simplify the notation). Then, in the second step, the subsets $\tilde{\mathcal{V}}_\ell^h$ and $\tilde{\mathcal{V}}_\ell^p$ are used to define subsets \mathcal{M}_ℓ^h and \mathcal{M}_ℓ^p of the set of marked simplices \mathcal{M}_ℓ^θ (see (3.5)). The subsets \mathcal{M}_ℓ^h and \mathcal{M}_ℓ^p are not necessarily disjoint which means that some simplices can be flagged for hp -refinement. Finally, the two subsets \mathcal{M}_ℓ^h and \mathcal{M}_ℓ^p are used to construct $\mathcal{T}_{\ell+1}$ and $\mathbf{p}_{\ell+1}$.

4.1. hp -decision on vertices

Our hp -decision on marked vertices is made on the basis of two local primal solves on the patch $\mathcal{T}_\ell^{\mathbf{a}}$ attached to each marked vertex $\mathbf{a} \in \tilde{\mathcal{V}}_\ell^\theta$. The idea

is to construct two distinct local patch-based spaces in order to emulate separately the effects of h - and p -refinement. Let us denote the polynomial-degree distribution in the patch $\mathcal{T}_\ell^{\mathbf{a}}$ by the vector $\mathbf{p}_\ell^{\mathbf{a}} := (p_{\ell,K})_{K \in \mathcal{T}_\ell^{\mathbf{a}}}$.

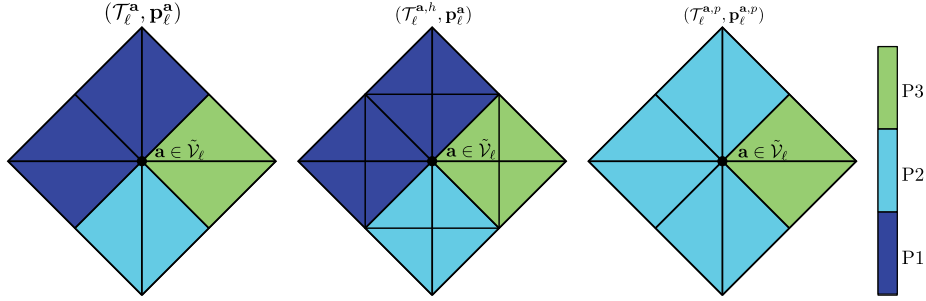


Figure 1: An example of patch $\mathcal{T}_\ell^{\mathbf{a}}$ together with its polynomial-degree distribution $\mathbf{p}_\ell^{\mathbf{a}}$ (left) and its h -refined (center) and p -refined versions (right) from Definitions 4.1 and 4.2 respectively.

Definition 4.1 (*h -refinement residual*). Let $\mathbf{a} \in \tilde{\mathcal{V}}_\ell^\theta$ be a marked vertex with associated patch $\mathcal{T}_\ell^{\mathbf{a}}$ and polynomial-degree distribution $\mathbf{p}_\ell^{\mathbf{a}}$. We set

$$V_\ell^{\mathbf{a},h} := \mathbb{P}_{\mathbf{p}_\ell^{\mathbf{a},h}}(\mathcal{T}_\ell^{\mathbf{a},h}) \cap H_0^1(\omega_\ell^{\mathbf{a}}), \quad (4.1)$$

where $\mathcal{T}_\ell^{\mathbf{a},h}$ is obtained as a matching simplicial refinement of $\mathcal{T}_\ell^{\mathbf{a}}$ by dividing each simplex $K \in \mathcal{T}_\ell^{\mathbf{a}}$ into at least two children simplices, and the polynomial-degree distribution $\mathbf{p}_\ell^{\mathbf{a},h}$ is obtained from $\mathbf{p}_\ell^{\mathbf{a}}$ by assigning to each newly-created simplex the same polynomial degree as its parent. Then, we let $r^{\mathbf{a},h} \in V_\ell^{\mathbf{a},h}$ solve

$$(\nabla r^{\mathbf{a},h}, \nabla v^{\mathbf{a},h})_{\omega_\ell^{\mathbf{a}}} = (f, v^{\mathbf{a},h})_{\omega_\ell^{\mathbf{a}}} - (\nabla u_\ell, \nabla v^{\mathbf{a},h})_{\omega_\ell^{\mathbf{a}}} \quad \forall v^{\mathbf{a},h} \in V_\ell^{\mathbf{a},h}.$$

Definition 4.2 (*p -refinement residual*). Let $\mathbf{a} \in \tilde{\mathcal{V}}_\ell^\theta$ be a marked vertex with associated patch $\mathcal{T}_\ell^{\mathbf{a}}$ and polynomial-degree distribution $\mathbf{p}_\ell^{\mathbf{a}}$. We set

$$V_\ell^{\mathbf{a},p} := \mathbb{P}_{\mathbf{p}_\ell^{\mathbf{a},p}}(\mathcal{T}_\ell^{\mathbf{a},p}) \cap H_0^1(\omega_\ell^{\mathbf{a}}), \quad (4.2)$$

where $\mathcal{T}_\ell^{\mathbf{a},p} := \mathcal{T}_\ell^{\mathbf{a}}$, and the polynomial-degree distribution $\mathbf{p}_\ell^{\mathbf{a},p}$ is obtained from $\mathbf{p}_\ell^{\mathbf{a}}$ by assigning to each simplex $K \in \mathcal{T}_\ell^{\mathbf{a},p} = \mathcal{T}_\ell^{\mathbf{a}}$ the polynomial degree $p_{\ell,K} + \delta_K^{\mathbf{a}}$

where

$$\delta_K^{\mathbf{a}} := \begin{cases} 1 & \text{if } p_{\ell, K} = \min_{K' \in \mathcal{T}_\ell^{\mathbf{a}}} p_{\ell, K'}, \\ 0 & \text{otherwise.} \end{cases} \quad (4.3)$$

Then, we let $r^{\mathbf{a}, p} \in V_\ell^{\mathbf{a}, p}$ solve

$$(\nabla r^{\mathbf{a}, p}, \nabla v^{\mathbf{a}, p})_{\omega_\ell^{\mathbf{a}}} = (f, v^{\mathbf{a}, p})_{\omega_\ell^{\mathbf{a}}} - (\nabla u_\ell, \nabla v^{\mathbf{a}, p})_{\omega_\ell^{\mathbf{a}}} \quad \forall v^{\mathbf{a}, p} \in V_\ell^{\mathbf{a}, p}.$$

The local residual liftings $r^{\mathbf{a}, h}$ and $r^{\mathbf{a}, p}$ from Definitions 4.1 and 4.2, respectively, are used to define the following two disjoint subsets of the set of marked vertices $\tilde{\mathcal{V}}_\ell^\theta$:

$$\tilde{\mathcal{V}}_\ell^h := \{\mathbf{a} \in \tilde{\mathcal{V}}_\ell^\theta \mid \|\nabla r^{\mathbf{a}, h}\|_{\omega_\ell^{\mathbf{a}}} \geq \|\nabla r^{\mathbf{a}, p}\|_{\omega_\ell^{\mathbf{a}}}\}, \quad (4.4a)$$

$$\tilde{\mathcal{V}}_\ell^p := \{\mathbf{a} \in \tilde{\mathcal{V}}_\ell^\theta \mid \|\nabla r^{\mathbf{a}, h}\|_{\omega_\ell^{\mathbf{a}}} < \|\nabla r^{\mathbf{a}, p}\|_{\omega_\ell^{\mathbf{a}}}\}, \quad (4.4b)$$

in such a way that

$$\tilde{\mathcal{V}}_\ell^\theta = \tilde{\mathcal{V}}_\ell^h \cup \tilde{\mathcal{V}}_\ell^p, \quad \tilde{\mathcal{V}}_\ell^h \cap \tilde{\mathcal{V}}_\ell^p = \emptyset.$$

The above hp -decision criterion on vertices means that a marked vertex is flagged for h -refinement if the local residual norm $\|\nabla r^{\mathbf{a}, h}\|_{\omega_\ell^{\mathbf{a}}}$ is larger than $\|\nabla r^{\mathbf{a}, p}\|_{\omega_\ell^{\mathbf{a}}}$; otherwise, this vertex is flagged for p -refinement. Further motivation for this choice is discussed in Remark 5.3 below.

170 **Remark 4.3** (p -refinement). *Other choices are possible for the polynomial-degree increment defined in (4.3). One possibility is to set $\delta_K^{\mathbf{a}} = 1$ for all $K \in \mathcal{T}_\ell^{\mathbf{a}}$. However, in our numerical experiments, we observe that this choice leads to rather scattered polynomial-degree distributions over the whole computational domain. The choice (4.3) is more conservative and leads to a smoother*
 175 *overall polynomial-degree distribution. We believe that this choice is preferable, at least as long as a polynomial-degree coarsening procedure is not included in the adaptive loop. Another possibility is to use $\lceil \alpha p_{\ell, K} \rceil$ with $\alpha > 1$ instead of $p_{\ell, K} + \delta_K^{\mathbf{a}}$, which corresponds to the theoretical developments in [9].*

4.2. hp -decision on simplices

The second step in the module REFINE is to use the subsets $\tilde{\mathcal{V}}_\ell^h$ and $\tilde{\mathcal{V}}_\ell^p$ to decide whether h -, p -, or hp -refinement should be performed on each simplex

having at least one flagged vertex. To this purpose, we define the following subsets:

$$\mathcal{M}_\ell^h := \{K \in \mathcal{T}_\ell \mid \mathcal{V}_K \cap \tilde{\mathcal{V}}_\ell^h \neq \emptyset\} \subset \mathcal{M}_\ell^\theta, \quad (4.5a)$$

$$\mathcal{M}_\ell^p := \{K \in \mathcal{T}_\ell \mid \mathcal{V}_K \cap \tilde{\mathcal{V}}_\ell^p \neq \emptyset\} \subset \mathcal{M}_\ell^\theta. \quad (4.5b)$$

180 In other words, a simplex $K \in \mathcal{T}_\ell$ is flagged for h -refinement (resp., p -refinement) if it has at least one vertex flagged for h -refinement (resp., p -refinement). Note that the subsets \mathcal{M}_ℓ^h and \mathcal{M}_ℓ^p are not necessarily disjoint since a simplex can have some vertices flagged for h -refinement and others flagged for p -refinement; such simplices are then flagged for hp -refinement. Note also that $\mathcal{M}_\ell^h \cup \mathcal{M}_\ell^p =$
 185 $\cup_{\mathbf{a} \in \tilde{\mathcal{V}}_\ell^\theta} \mathcal{T}_\ell^\mathbf{a} = \mathcal{M}_\ell^\theta$ is indeed the set of marked simplices considered in the module MARK.

4.3. hp -refinement

In this last and final step, the subsets \mathcal{M}_ℓ^h and \mathcal{M}_ℓ^p are used to produce first the next mesh $\mathcal{T}_{\ell+1}$ and then the next polynomial-degree distribution $\mathbf{p}_{\ell+1}$ on
 190 the mesh $\mathcal{T}_{\ell+1}$.

The next mesh $\mathcal{T}_{\ell+1}$ is a matching simplicial refinement of \mathcal{T}_ℓ obtained by dividing each flagged simplex $K \in \mathcal{M}_\ell^h$ into at least two simplices in a way that is consistent with the matching simplicial refinement of $\mathcal{T}_\ell^\mathbf{a}$ considered in Definition 4.1 to build $\mathcal{T}_\ell^{\mathbf{a},h}$, i.e., such that $\mathcal{T}_\ell^{\mathbf{a},h} \subset \mathcal{T}_{\ell+1}$ for all $\mathbf{a} \in \tilde{\mathcal{V}}_\ell^h$. Note
 195 that to preserve the conformity of the mesh, additional refinements beyond the set of flagged simplices \mathcal{M}_ℓ^h may be carried out when building $\mathcal{T}_{\ell+1}$. Several algorithms can be considered to refine the mesh. In our numerical experiments, we used the newest vertex bisection algorithm [30].

After having constructed the next mesh $\mathcal{T}_{\ell+1}$, we assign the next polynomial-degree distribution $\mathbf{p}_{\ell+1}$ as follows. For all $\tilde{K} \in \mathcal{T}_{\ell+1}$, let K denote its parent simplex in \mathcal{T}_ℓ . We then set

$$p_{\ell+1, \tilde{K}} := p_{\ell, K} \quad \text{if } K \notin \mathcal{M}_\ell^p, \quad (4.6)$$

that is, we assign the same polynomial degree to the children of a simplex that is not flagged for p -refinement, whereas we set

$$p_{\ell+1, \tilde{K}} := \max_{\mathbf{a} \in \mathcal{V}_K \cap \tilde{\mathcal{V}}_\ell^p} (p_{\ell, K} + \delta_K^{\mathbf{a}}) \quad \text{if } K \in \mathcal{M}_\ell^p, \quad (4.7)$$

that is, we assign to the children of a simplex $K \in \mathcal{M}_\ell^p$ flagged for p -refinement the largest of the polynomial degrees considered in Definition 4.2 to build the local residual liftings associated with the vertices of K flagged for p -refinement.

4.4. Summary of the module REFINE

The module REFINE is summarized in Algorithm 2.

Algorithm 2 (module REFINE)

```

1: module REFINE( $\tilde{\mathcal{V}}_\ell^\theta$ )
2:    $\triangleright$  Input: set of marked vertices  $\tilde{\mathcal{V}}_\ell^\theta$ 
3:    $\triangleright$  Output: next level mesh  $\mathcal{T}_{\ell+1}$ , polynomial-degree distribution  $\mathbf{p}_{\ell+1}$ 
4:   for all  $\mathbf{a} \in \tilde{\mathcal{V}}_\ell^\theta$  do
5:     Compute the  $h$ -refinement residual lifting  $r^{\mathbf{a}, h}$  from Definition 4.1
6:     Compute the  $p$ -refinement residual lifting  $r^{\mathbf{a}, p}$  from Definition 4.2
7:   end for
8:    $hp$ -decision on vertices: build the subsets  $\tilde{\mathcal{V}}_\ell^h$  and  $\tilde{\mathcal{V}}_\ell^p$  from (4.4)
9:    $hp$ -decision on simplices: build the subsets  $\mathcal{M}_\ell^h$  and  $\mathcal{M}_\ell^p$  from (4.5)
10:  Build  $\mathcal{T}_{\ell+1}$  from  $\mathcal{T}_\ell$  and  $\mathcal{M}_\ell^h$ 
11:  Build  $\mathbf{p}_{\ell+1}$  on  $\mathcal{T}_{\ell+1}$  from  $\mathbf{p}_\ell$ ,  $\{\delta_K^{\mathbf{a}}\}_{\mathbf{a} \in \tilde{\mathcal{V}}_\ell^p, K \in \mathcal{T}_\ell^p}$ , and  $\mathcal{M}_\ell^p$  using (4.6)
    and (4.7)
12: end module

```

To illustrate Algorithm 2, we examine in detail a particular situation with three marked vertices as encountered on the 6th iteration ($\ell = 6$) of the adaptive loop applied to the L-shape problem described in Section 6.2 below. In Figure 2 (left panel), we display the mesh \mathcal{T}_6 and the polynomial-degree distribution \mathbf{p}_6 . There are three marked vertices in $\tilde{\mathcal{V}}_6^\theta$. In Figure 3, for the three marked vertices, we visualize the norms $\|\nabla r^{\mathbf{a}, h}\|_{\omega_6^{\mathbf{a}}}$ and $\|\nabla r^{\mathbf{a}, p}\|_{\omega_6^{\mathbf{a}}}$ which are the key

210 ingredients for the hp -decision on vertices. The resulting simplices flagged for h - and p -refinement are shown in the central panel of Figure 2, whereas the right panel of Figure 2 displays the next mesh \mathcal{T}_7 and the next polynomial-degree distribution \mathbf{p}_7 .

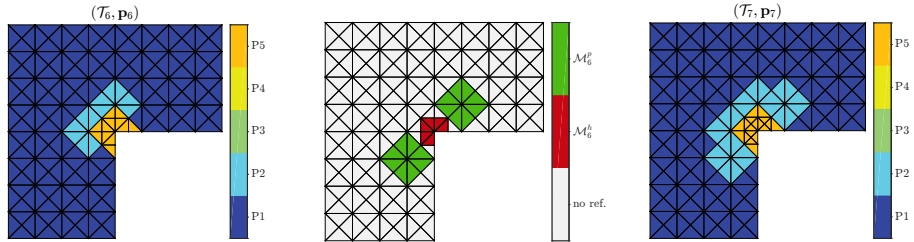


Figure 2: [L-shape problem from Section 6.2] The mesh and the polynomial degree distribution on the 6th iteration of the adaptive procedure (*left*). Result of the hp -decision: simplices in \mathcal{M}_6^h are shown in blue and simplices in \mathcal{M}_6^p are shown in red, the two subsets \mathcal{M}_6^h and \mathcal{M}_6^p being here disjoint (*center*). The resulting mesh \mathcal{T}_7 and polynomial-degree distribution \mathbf{p}_7 (*right*).

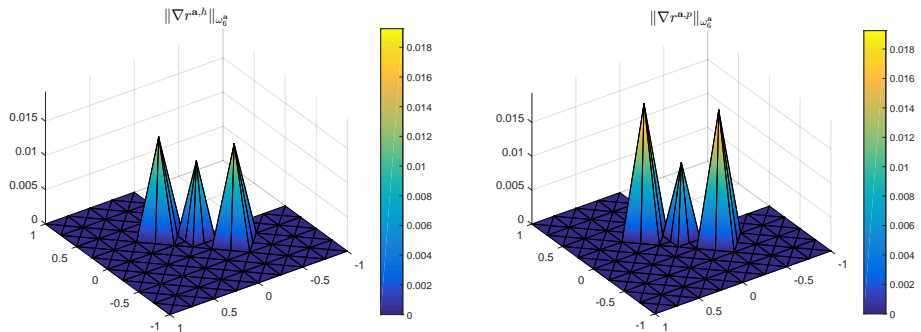


Figure 3: [L-shape problem from Section 6.2] For the three marked vertices in $\tilde{\mathcal{V}}_6^\emptyset$, we display the piecewise \mathbb{P}_1 functions which take the value $\|\nabla r^{\mathbf{a},h}\|_{\omega_6^{\mathbf{a}}}$ in the vertex \mathbf{a} and 0 elsewhere (*left*) and the value $\|\nabla r^{\mathbf{a},p}\|_{\omega_6^{\mathbf{a}}}$ in the vertex \mathbf{a} and 0 elsewhere (*right*).

5. Guaranteed bound on the error reduction factor

215 In this section we show that it is possible to compute, at marginal additional costs, a guaranteed bound on the energy error reduction factor C_{red} from (1.3)

on each iteration ℓ of the adaptive loop (1.2). This bound can be computed right after the end of module REFINE at the modest price of one additional primal solve in each patch $\mathcal{T}_\ell^{\mathbf{a}}$ associated with each marked vertex $\mathbf{a} \in \tilde{\mathcal{V}}_\ell^\theta$. Recall the set of marked simplices $\mathcal{M}_\ell^\theta = \cup_{\mathbf{a} \in \tilde{\mathcal{V}}_\ell^\theta} \mathcal{T}_\ell^{\mathbf{a}}$. Let us denote by $\omega_\ell := \cup_{\mathbf{a} \in \tilde{\mathcal{V}}_\ell^\theta} \omega_\ell^{\mathbf{a}}$ the corresponding open subdomain; notice that a point \mathbf{x} is in $\overline{\omega_\ell}$ if and only if there is $K \in \mathcal{M}_\ell^\theta$ so that $\mathbf{x} \in K$. We start with the following discrete lower bound result:

Lemma 5.1 (Guaranteed lower bound on the incremental error on marked simplices). *Let the mesh $\mathcal{T}_{\ell+1}$ and the polynomial-degree distribution $\mathbf{p}_{\ell+1}$ result from Algorithm 2, and recall that $V_{\ell+1} = \mathbb{P}_{\mathbf{p}_{\ell+1}}(\mathcal{T}_{\ell+1}) \cap H_0^1(\Omega)$ is the finite element space to be used on iteration $(\ell + 1)$ of the adaptive loop (1.2). For all the marked vertices $\mathbf{a} \in \tilde{\mathcal{V}}_\ell^\theta$, let us set, in extension of (4.1), (4.2),*

$$V_\ell^{\mathbf{a},hp} := V_{\ell+1}|_{\omega_\ell^{\mathbf{a}}} \cap H_0^1(\omega_\ell^{\mathbf{a}}),$$

and construct the residual lifting $r^{\mathbf{a},hp} \in V_\ell^{\mathbf{a},hp}$ by solving

$$(\nabla r^{\mathbf{a},hp}, \nabla v^{\mathbf{a},hp})_{\omega_\ell^{\mathbf{a}}} = (f, v^{\mathbf{a},hp})_{\omega_\ell^{\mathbf{a}}} - (\nabla u_\ell, \nabla v^{\mathbf{a},hp})_{\omega_\ell^{\mathbf{a}}} \quad \forall v^{\mathbf{a},hp} \in V_\ell^{\mathbf{a},hp}. \quad (5.1)$$

Then, extending $r^{\mathbf{a},hp}$ by zero outside $\omega_\ell^{\mathbf{a}}$, the following holds true:

$$\|\nabla(u_{\ell+1} - u_\ell)\|_{\omega_\ell} \geq \underline{\eta}_{\mathcal{M}_\ell^\theta}, \quad \underline{\eta}_{\mathcal{M}_\ell^\theta} := \begin{cases} \frac{\sum_{\mathbf{a} \in \tilde{\mathcal{V}}_\ell^\theta} \|\nabla r^{\mathbf{a},hp}\|_{\omega_\ell^{\mathbf{a}}}^2}{\left\| \nabla \left(\sum_{\mathbf{a} \in \tilde{\mathcal{V}}_\ell^\theta} r^{\mathbf{a},hp} \right) \right\|_{\omega_\ell}} & \text{if } \sum_{\mathbf{a} \in \tilde{\mathcal{V}}_\ell^\theta} r^{\mathbf{a},hp} \neq 0, \\ 0 & \text{otherwise.} \end{cases} \quad (5.2)$$

Proof. Let $V_{\ell+1}(\omega_\ell)$ stand for the restriction of the space $V_{\ell+1}$ to the subdomain ω_ℓ and let $V_{\ell+1}^0(\omega_\ell) := V_{\ell+1}(\omega_\ell) \cap H_0^1(\omega_\ell)$ stand for the corresponding homogeneous Dirichlet subspace. Note that $(u_{\ell+1} - u_\ell)$ is a member of $V_{\ell+1}(\omega_\ell)$, but

not necessarily of $V_{\ell+1}^0(\omega_\ell)$. Then, the following holds true:

$$\begin{aligned} \|\nabla(u_{\ell+1} - u_\ell)\|_{\omega_\ell} &= \sup_{v_{\ell+1} \in V_{\ell+1}(\omega_\ell)} \frac{(\nabla(u_{\ell+1} - u_\ell), \nabla v_{\ell+1})_{\omega_\ell}}{\|\nabla v_{\ell+1}\|_{\omega_\ell}} \\ &\geq \sup_{v_{\ell+1} \in V_{\ell+1}^0(\omega_\ell)} \frac{(\nabla(u_{\ell+1} - u_\ell), \nabla v_{\ell+1})_{\omega_\ell}}{\|\nabla v_{\ell+1}\|_{\omega_\ell}} \\ &= \sup_{v_{\ell+1} \in V_{\ell+1}^0(\omega_\ell)} \frac{(f, v_{\ell+1})_{\omega_\ell} - (\nabla u_\ell, \nabla v_{\ell+1})_{\omega_\ell}}{\|\nabla v_{\ell+1}\|_{\omega_\ell}}, \end{aligned}$$

where we have used the definition (3.1) of $u_{\ell+1}$ on the mesh $\mathcal{T}_{\ell+1}$, since $v_{\ell+1}$ extended by zero outside of ω_ℓ belongs to the space $V_{\ell+1}$ whenever $v_{\ell+1} \in V_{\ell+1}^0(\omega_\ell)$. Now, choosing $v_{\ell+1} = \sum_{\mathbf{a} \in \tilde{\mathcal{V}}_\ell^\theta} r^{\mathbf{a}, hp}$ (note that this function indeed belongs to $V_{\ell+1}^0(\omega_\ell)$), we infer that

$$\begin{aligned} \left(f, \sum_{\mathbf{a} \in \tilde{\mathcal{V}}_\ell^\theta} r^{\mathbf{a}, hp} \right)_{\omega_\ell} - \left(\nabla u_\ell, \nabla \left(\sum_{\mathbf{a} \in \tilde{\mathcal{V}}_\ell^\theta} r^{\mathbf{a}, hp} \right) \right)_{\omega_\ell} \\ = \sum_{\mathbf{a} \in \tilde{\mathcal{V}}_\ell^\theta} \left\{ (f, r^{\mathbf{a}, hp})_{\omega_\ell^\mathbf{a}} - (\nabla u_\ell, \nabla r^{\mathbf{a}, hp})_{\omega_\ell^\mathbf{a}} \right\} = \sum_{\mathbf{a} \in \tilde{\mathcal{V}}_\ell^\theta} \|\nabla r^{\mathbf{a}, hp}\|_{\omega_\ell^\mathbf{a}}^2, \end{aligned}$$

where we have employed $r^{\mathbf{a}, hp}$ as a test function in (5.1). This finishes the
225 proof. □

Our main result is summarized in the following contraction property in the spirit of [12, Theorem 5.1], [9, Proposition 4.1], and the references therein. The specificity of the present work is that we obtain a guaranteed and computable bound on the error reduction factor. In contrast to these references, however,
230 we do not prove here that C_{red} is strictly smaller than one, although we observe it numerically in Section 6 below. We believe that one could show $C_{\text{red}} < 1$ under additional assumptions on the refinements, such as the interior node property [27], but we will not pursue this consideration further here.

Theorem 5.2 (Guaranteed bound on the energy error reduction factor). *Let the mesh $\mathcal{T}_{\ell+1}$ and the polynomial-degree distribution $\mathbf{p}_{\ell+1}$ result from Algorithm 2, and let $V_{\ell+1} = \mathbb{P}_{\mathbf{p}_{\ell+1}}(\mathcal{T}_{\ell+1}) \cap H_0^1(\Omega)$ be the finite element space to be used on iteration $(\ell + 1)$ of the adaptive loop (1.2). Let $\underline{\eta}_{\mathcal{M}_\ell^\theta}$ be defined by (5.2). Then,*

unless $\eta(\mathcal{M}_\ell^\theta) = 0$ in which case $u_\ell = u$ and the adaptive loop terminates, the new numerical solution $u_{\ell+1} \in V_{\ell+1}$ satisfies

$$\|\nabla(u - u_{\ell+1})\| \leq C_{\text{red}} \|\nabla(u - u_\ell)\| \quad \text{with} \quad 0 \leq C_{\text{red}} := \sqrt{1 - \theta^2 \frac{\underline{\eta}_{\mathcal{M}_\ell^\theta}^2}{\eta^2(\mathcal{M}_\ell^\theta)}} \leq 1. \quad (5.3)$$

Proof. We first observe that $\eta(\mathcal{M}_\ell^\theta) = 0$ implies using (3.4) and (3.3) that the error is zero on iteration ℓ , i.e., $u = u_\ell$, so that the adaptive loop (1.2) terminates. Let us now assume that $\eta(\mathcal{M}_\ell^\theta) \neq 0$. Since the spaces $\{V_\ell\}_{\ell \geq 0}$ are nested, cf. (2.1), Galerkin's orthogonality implies the following Pythagorean identity:

$$\|\nabla(u - u_{\ell+1})\|^2 = \|\nabla(u - u_\ell)\|^2 - \|\nabla(u_{\ell+1} - u_\ell)\|^2.$$

Moreover, owing to Lemma 5.1, we infer that

$$\|\nabla(u_{\ell+1} - u_\ell)\| \geq \|\nabla(u_{\ell+1} - u_\ell)\|_{\omega_\ell} \geq \underline{\eta}_{\mathcal{M}_\ell^\theta} = \frac{\underline{\eta}_{\mathcal{M}_\ell^\theta}}{\eta(\mathcal{M}_\ell^\theta)} \eta(\mathcal{M}_\ell^\theta).$$

Using the marking criterion (3.4) and the definition of \mathcal{M}_ℓ^θ , we next see that

$$\begin{aligned} \|\nabla(u - u_{\ell+1})\|^2 &\leq \|\nabla(u - u_\ell)\|^2 - \frac{\underline{\eta}_{\mathcal{M}_\ell^\theta}^2}{\eta^2(\mathcal{M}_\ell^\theta)} \eta^2(\mathcal{M}_\ell^\theta) \\ &\leq \|\nabla(u - u_\ell)\|^2 - \theta^2 \frac{\underline{\eta}_{\mathcal{M}_\ell^\theta}^2}{\eta^2(\mathcal{M}_\ell^\theta)} \eta^2(\mathcal{T}_\ell). \end{aligned}$$

The assertion (5.3) follows from the error estimate (3.3) and taking the square root. □

Remark 5.3 (Local residual optimization). *The use of the local residual liftings $r^{\mathbf{a},h}$ and $r^{\mathbf{a},p}$ from Definitions 4.1 and 4.2 respectively in the hp-decision criterion (4.4) on marked vertices is motivated by the result of Theorem 5.2. Indeed, suppose that $r^{\mathbf{a},h}$ is larger than $r^{\mathbf{a},p}$ in norm, and that only h-refinement is performed in the subdomain $\omega_\ell^{\mathbf{a}}$ at the end of Algorithm 2. Then, the local residual $r^{\mathbf{a},hp}$ from Lemma 5.1 coincides with $r^{\mathbf{a},h}$ which means that by flagging the marked vertex \mathbf{a} for h-refinement, one maximizes the contribution $\|\nabla r^{\mathbf{a},hp}\|_{\omega_\ell^{\mathbf{a}}}^2$ in the numerator of (5.2) defining $\underline{\eta}_{\mathcal{M}_\ell^\theta}$. It is also possible to design a more*

complex hp -refinement strategy exploiting directly (5.3). Here we simply stick
 245 to Algorithm 2 which in our numerical experiments reported in Section 6 below
 leads to exponential convergence rates.

Remark 5.4 (A sharper bound). Theorem 5.2 obviously also holds true with the
 slightly sharper constant $C_{\text{red}} = \sqrt{1 - \frac{\eta^2 \mathcal{M}_\ell^\theta}{\eta^2(\mathcal{T}_\ell)}}$. This is equivalent to considering
 in (5.3) θ_ℓ such that $\eta(\mathcal{M}_\ell^\theta) = \theta_\ell \eta(\mathcal{T}_\ell)$ in place of θ , a strategy adopted in
 250 the numerical experiments in Section 6 below. We note that $\theta_\ell \geq \theta$, however
 employing θ_ℓ in Algorithm 1 would lead to the same set of marked simplices
 $\mathcal{M}_\ell^{\theta_\ell} = \mathcal{M}_\ell^\theta$.

6. Numerical experiments

We consider two test cases for the model problem (1.1), both in two space
 dimensions, one with a (relatively) smooth weak solution and one with a singu-
 lar weak solution. Our main goal with the numerical experiments is to verify
 that the hp -refinement strategy of Algorithm 2 leads to an exponential rate of
 convergence with respect to the number of degrees of freedom DoF_ℓ of the finite
 element spaces V_ℓ in the form

$$\|\nabla(u - u_\ell)\| \leq C_1 \exp\left(-C_2 \text{DoF}_\ell^{\frac{1}{3}}\right), \quad (6.1)$$

with positive constants C_1, C_2 independent of DoF_ℓ . In addition, we assess
 the sharpness of the guaranteed bound on the reduction factor C_{red} from The-
 orem 5.2 by means of the effectivity index defined as

$$I_{\text{red}}^{\text{eff}} = \frac{C_{\text{red}}}{\frac{\|\nabla(u - u_{\ell+1})\|}{\|\nabla(u - u_\ell)\|}}. \quad (6.2)$$

We always consider the (well-established) choice $\theta = 0.5$ for the marking pa-
 255 rameter, fine-tuning it on each step to θ_ℓ as described in Remark 5.4. As men-
 tioned above, we apply the newest vertex bisection algorithm [30] to perform
 h -refinement and we use the polynomial-degree increment (4.3) to perform p -
 refinement.

We compare the performance of our hp -refinement algorithm to two other
260 algorithms based on a different hp -decision criteria, namely the PARAM and
PRIOR criteria from the survey paper [26] which are both based on a local
smoothness estimation. These criteria hinge on the local L^2 -orthogonal projec-
tion u_ℓ^{p-1} of the numerical solution u_ℓ onto the local lower-polynomial-degree
space $\mathbb{P}_{p_{\ell,K}-1}(K)$ for all the marked simplices $K \in \mathcal{M}_\ell^g$. This leads to the local
265 quantity $\eta_K^{p-1} := \|\nabla(u_\ell - u_\ell^{p-1})\|_K$; in case of $p_{\ell,K} = 1$, when the quantity η_K^{p-1}
is not available, for both criteria, the marked simplex K is p -refined. The crite-
rion PARAM [22] relies on the local smoothness indicator $g_K := \eta_K/\eta_K^{p-1}$ and a
user-defined parameter $\gamma > 0$; the marked simplex K is h -refined if $g_K > \gamma$, and
otherwise it is p -refined. The presence of the parameter γ is a drawback of this
270 criterion; in our experiments we use the values $\gamma = 0.3$ and $\gamma = 0.6$, as suggested
in [26]. The criterion PRIOR, which is a simplified version of the one proposed
in [32], relies on the quantity $s_K := 1 - \log(\eta_K/\eta_K^{p-1})/\log(p_{\ell,K}/(p_{\ell,K} - 1))$;
the marked simplex K is h -refined if $p_{\ell,K} > s_K - 1$, and otherwise it is p -
refined. To make the comparison with our approach more objective, we apply
275 for both criteria the suggested p -refinement only to those simplices such that
 $p_{\ell,K} = \min_{K' \in \mathcal{T}_a} p_{\ell,K'}$.

6.1. Smooth solution (sharp Gaussian)

We consider a square domain $\Omega = (-1, 1) \times (-1, 1)$ and a weak solution that
is smooth but has a rather sharp peak

$$u(x, y) = (x^2 - 1)(y^2 - 1) \exp(-100(x^2 + y^2)).$$

We start from a criss-cross initial mesh \mathcal{T}_0 with $\max_{K \in \mathcal{T}_0} h_K = 0.25$ and a
uniform polynomial-degree distribution equal to 1 on all triangles.

280 Figure 4 presents the final mesh and polynomial-degree distribution obtained
after 30 steps of the hp -adaptive procedure (1.2) (left panel) along with the ob-
tained numerical solution (right panel). Figure 5 displays the relative error
 $\|\nabla(u - u_\ell)\|/\|\nabla u\|$ as a function of $\text{DoF}_\ell^{\frac{1}{3}}$ in logarithmic-linear scale to illus-
trate that the present hp -adaptive procedure leads to an asymptotic exponential

285 rate of convergence. The values of the constants C_1 and C_2 from (6.1) given
 by the 2-parameter least squares fit are 3.97 and 0.70, respectively. The value
 of C_2 indicates the slope steepness of the fitted line in logarithmic-linear scale,
 in particular, the higher value of C_2 , the steeper slope. For comparison, we
 also plot the relative error obtained when using the hp -decision criteria PRIOR
 290 and PARAM described above and also for the pure h -version of the adaptive
 loop. The quality of the a posteriori error estimators of Theorem 3.2 through-
 out the whole hp -adaptive process can be appreciated in Figure 6 where the
 effectivity indices, defined as the ratio of the error estimator $\eta(\mathcal{T}_\ell)$ and the ac-
 tual error $\|\nabla(u - u_\ell)\|$, are presented. Then, in Figure 7 we compare the actual
 295 and estimated error distributions on iteration $\ell = 20$ of the adaptive loop, show-
 ing excellent agreement. Figure 8 (left panel) presents the effectivity index for
 the reduction factor C_{red} , see (6.2), throughout the adaptive process. Overall,
 values quite close to one are obtained, except at some of the first iterations
 where the values are larger but do not exceed 2.5. Moreover, all the values
 300 are larger than one, confirming that the bound on the reduction factor C_{red} is
 indeed guaranteed. Figure 8 (right panel) examines the quality of the lower
 bound $\underline{\eta}_{\mathcal{M}_\ell^\theta}$ from Lemma 5.1 by plotting the ratio of the left-hand side to the
 right-hand side of the lower bound in (5.2). Except for one iteration where this
 ratio takes a larger value close to 4.5, we observe that this ratio takes always
 305 values quite close to, and larger than, one, indicating that $\underline{\eta}_{\mathcal{M}_\ell^\theta}$ delivers a sharp
 and guaranteed lower bound on the energy error decrease. To give some further
 insight into the proposed hp -adaptive process, we present in Tables 1 and 2
 some details on the hp -refinement decisions throughout the first 10 and the last
 10 iterations of the adaptive loop. Finally, Table 5 (top) compares the different
 310 strategies namely in terms of the number of iterations of the adaptive loop (1.2);
 here our strategy is a clear winner.

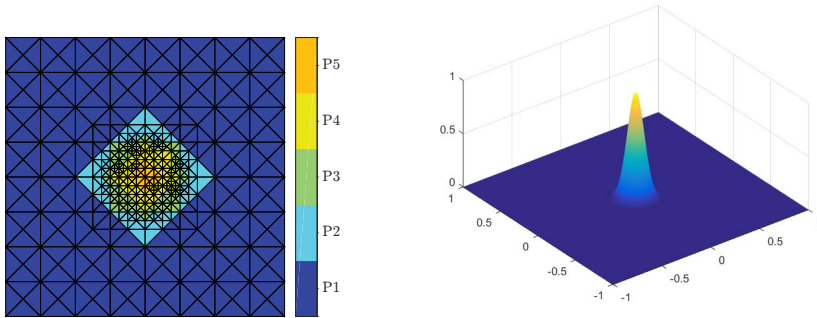


Figure 4: [Sharp-Gaussian of Section 6.1] The final mesh and polynomial-degree distribution obtained after 30 iterations of the hp -adaptive procedure (*left*) and the obtained numerical solution u_{30} (*right*).

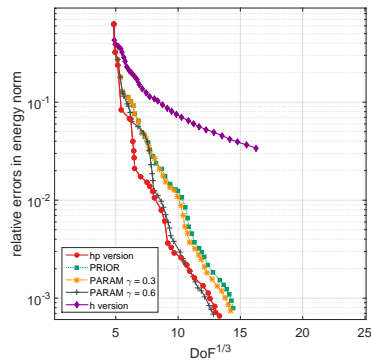


Figure 5: [Sharp-Gaussian of Section 6.1] Relative energy error $\|\nabla(u-u_\ell)\|/\|\nabla u\|$ as a function of $\text{DoF}_\ell^{\frac{1}{3}}$, obtained using the present hp -decision criterion, the criteria PRIOR and PARAM ($\gamma = 0.3$, $\gamma = 0.6$), and using only h -refinement.

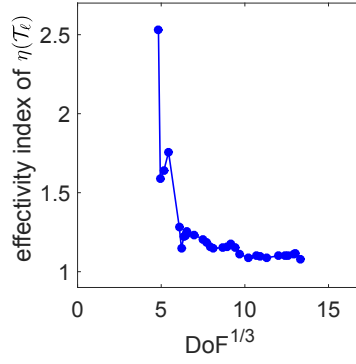


Figure 6: [Sharp-Gaussian of Section 6.1] Effectivity indices of the error estimators $\eta(\mathcal{T}_\ell)$ from Theorem 3.2, defined as the ratio $\eta(\mathcal{T}_\ell)/\|\nabla(u - u_\ell)\|$, throughout the hp -adaptive procedure.

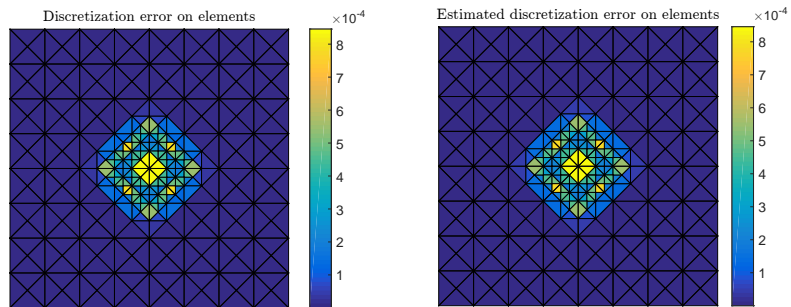


Figure 7: [Sharp-Gaussian of Section 6.1] The distribution of the energy error $\|\nabla(u - u_\ell)\|_K$ (left) and of the error estimators η_K from Theorem 3.2 (right), $\ell = 20$. The effectivity index of the estimate defined as $\eta(\mathcal{T}_{20})/\|\nabla(u - u_{20})\|$ is 1.1108.

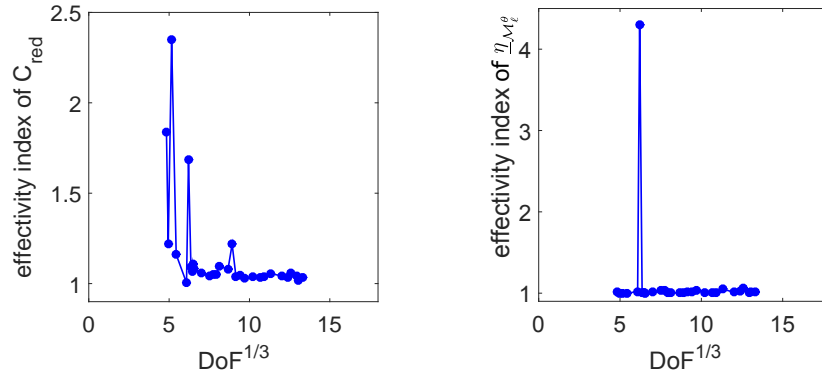


Figure 8: [Sharp-Gaussian of Section 6.1] Effectivity indices (6.2) for the error reduction factor C_{red} from Theorem 5.2 (*left*) and effectivity indices for the lower bound $\eta_{\mathcal{M}_\ell^\varrho}$ from Lemma 5.1 defined as the ratio $\|\nabla(u_{\ell+1} - u_\ell)\|_{\omega_\ell} / \eta_{\mathcal{M}_\ell^\varrho}$ (*right*).

Iteration	1	2	3	4	5	6	7	8	9	10
Triangles	256	256	256	256	264	264	264	264	264	264
Maximal polynomial degree	1	2	3	4	4	4	4	4	4	4
Marked vertices	1	1	1	1	2	2	2	1	1	1
Triangles flagged for h -refinement	0	0	0	8	0	0	0	0	0	8
Triangles flagged for p -refinement	8	8	8	0	12	12	4	2	2	0
Triangles flagged for hp -refinement	0	0	0	0	0	0	0	0	0	0

Table 1: [Sharp-Gaussian of Section 6.1] Refinement decisions in Algorithm 2 during the first 10 iterations of the adaptive loop (1.2).

Iteration	20	21	22	23	24	25	26	27	28	29
Triangles	392	406	430	450	478	514	552	580	612	612
Maximal polynomial degree	5	5	5	5	5	5	5	5	5	5
Marked vertices	2	3	3	3	4	3	2	3	4	4
Triangles flagged for h -refinement	12	24	16	24	30	23	14	21	0	28
Triangles flagged for p -refinement	0	0	4	0	0	0	0	0	16	0
Triangles flagged for hp -refinement	0	0	0	0	0	0	0	0	0	0

Table 2: [Sharp-Gaussian of Section 6.1] Refinement decisions in Algorithm 2 during the last 10 iterations of the adaptive loop (1.2).

6.2. Singular solution (L-shape domain)

In our second test case, we consider the L-shape domain $\Omega = (-1, 1) \times (-1, 1) \setminus [0, 1] \times [-1, 0]$ with $f = 0$ and the exact solution (in polar coordinates)

$$u(r, \varphi) = r^{\frac{2}{3}} \sin\left(\frac{2\varphi}{3}\right).$$

315 For this test case, following [15, Theorem 3.3] and the references therein, the error estimator $\eta(\mathcal{T}_\ell)$ employed within the adaptive procedure takes into account also the error from the approximation of the inhomogeneous Dirichlet boundary condition prescribed by the exact solution on $\partial\Omega$. We start the computation on a criss-cross grid \mathcal{T}_0 with $\max_{K \in \mathcal{T}_0} h_K = 0.25$ and all the polynomial degrees
320 set uniformly to 1.

Figure 9 presents the final mesh and polynomial-degree distribution after 65 steps of the hp -adaptive procedure (1.2) (left panel) along with a zoom in the window $[-10^{-6}, 10^{-6}] \times [-10^{-6}, 10^{-6}]$ near the re-entrant corner (right panel). Figure 10 (left panel) displays the relative error $\|\nabla(u - u_\ell)\|/\|\nabla u\|$ as a function of $\text{DoF}_\ell^{1/3}$ in logarithmic-linear scale to illustrate that, as in the previous test case, the present hp -adaptive procedure leads to an asymptotic exponential rate of convergence. The corresponding values of constants C_1 and C_2 in expression (6.1) obtained by the 2-parameter least squares fit are 4.73 and 0.69, respectively. For the direct comparison with other methods, we refer to the long version [25, Table 15] of the survey paper [26]. However, note that data sets of greater sizes than in our case have been used for the least squares fitting therein. A detailed view when the error takes lower values is provided in the right panel of Figure 10. We also plot the relative errors obtained when using the hp -decision criteria PRIOR and PARAM, as well as those obtained using APRIORI criterion exploiting the a priori knowledge of the exact solution (marked simplices are h -refined only if they touch the corner singularity, otherwise they are p -refined). In addition, we provide also the relative errors obtained by employing the (non-adaptive) strategy which we refer to as LINEAR, inspired by the theoretical results for the one-dimensional problem with singular solution [21, 22, 33]. When employing this strategy, we start from a

coarse grid \mathcal{T}_0 with $\max_{K \in \mathcal{T}_0} h_K = 0.5$. At each iteration, only the patch containing the re-entrant corner is h -refined. Thus, the elements of each mesh \mathcal{T}_ℓ , $\ell \geq 1$, decrease in size in geometric progression (in our case with factor 0.5) toward the re-entrant corner. For each \mathcal{T}_ℓ , $\ell \geq 1$, we group the elements in layers $\mathcal{L}_1, \mathcal{L}_2, \dots, \mathcal{L}_{m(\ell)}$ depending on their distance from the origin (\mathcal{L}_1 containing the singularity), such that $\mathcal{T}_\ell = \bigcup_{i=1}^{m(\ell)} \mathcal{L}_i$. The total number of layers $m(\ell)$ depends on how many times the current mesh \mathcal{T}_ℓ has been refined. Each element $K \in \mathcal{T}_\ell$ is then assigned polynomial degree $p_{\ell,K}$ layer-wise, increasing linearly away from the singularity, in the way

$$p_{\ell,K} := \left\lceil 1 + \frac{(i-1)}{3} \right\rceil,$$

where i is the index of the layer \mathcal{L}_i containing the element K . For the strategy APRIORI (Figure 11) and the strategy LINEAR (Figure 12), we illustrate also the resulting polynomial-degree distribution at the step when the relative error reaches 10^{-5} . As for the previous test case, in Figure 13 we illustrate the quality of the error estimator from Theorem 3.2 in terms of the effectivity index $\eta(\mathcal{T}_\ell)/\|\nabla(u-u_\ell)\|$ throughout all the iterations of the present hp -adaptive process. Figure 14 then compares the actual and estimated error distributions on iteration $\ell = 45$ of the adaptive loop, showing excellent agreement. Figure 15 (left panel) presents the effectivity index for the reduction factor C_{red} , see (6.2), throughout the adaptive process, whereas the right panel of Figure 15 examines the quality of the lower bound $\underline{\eta}_{\mathcal{M}_\ell^e}$ from Lemma 5.1 by plotting the ratio of the left-hand side to the right-hand side of the lower bound in (5.2). For both quantities, we can draw similar conclusions to the previous test case, thereby confirming that sharp estimates on the error reduction factor are available. Additional numerical experiments (not shown here) indicate that the lower bound estimate can be made even sharper by performing h -refinement so as to satisfy the interior node property. Finally, to give some further insight into the hp -adaptive process, we present in Tables 3 and 4 some details on the hp -refinement decisions made by the proposed hp -refinement criterion during the first 10 and the last 10 iterations of the adaptive loop. We observe that

in the initial iterations, where the underlying mesh is still rather coarse, the polynomial degree is increased also on those simplices touching the re-entrant corner. Nevertheless, this decision does not occur anymore later when the mesh around the singularity is already more strongly refined than in the rest of the domain. Therefore, an improvement of our approach is expected, as suggested in [8], in conjunction with an appropriate coarsening strategy correcting the excessive p -refinement in the early stages. Table 5 (bottom) again brings some additional comparisons with other strategies in terms of number of iterations and number of degrees of freedom necessary to reach relative error 10^{-5} . We observe that the results achieved using the present strategy are comparable with those achieved by other (established) strategies.

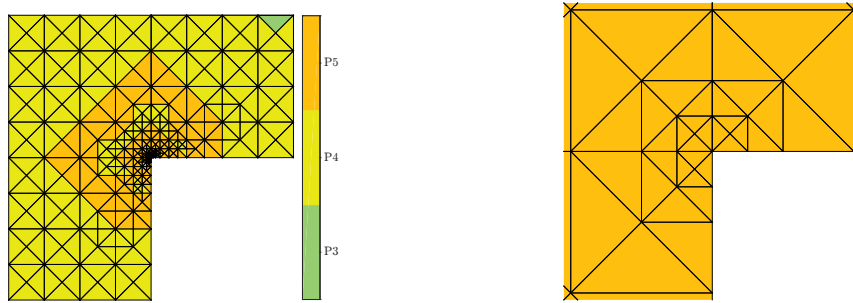


Figure 9: [L-shape domain of Section 6.2] The final mesh and polynomial-degree distribution obtained after 65 iterations of the hp -adaptive procedure (*left*) and a zoom in $[-10^{-6}, 10^{-6}] \times [-10^{-6}, 10^{-6}]$ near the re-entrant corner (*right*).

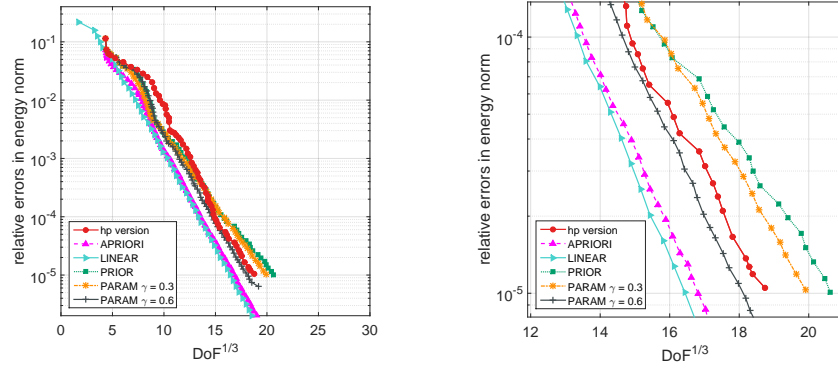


Figure 10: [L-shape domain of Section 6.2] Relative energy error $\|\nabla(u - u_\ell)\|/\|\nabla u\|$ as a function of $\text{DoF}_\ell^{1/3}$, obtained using the present hp -decision criterion, the criteria PRIOR and PARAM ($\gamma = 0.3$ and $\gamma = 0.6$), the APRIORI, and LINEAR strategy (*left*) and a detailed view (*right*).

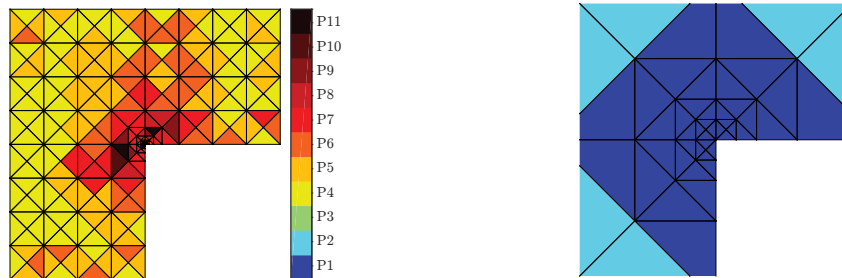


Figure 11: [L-shape domain of Section 6.2] Mesh and polynomial-degree distribution obtained after 70 iterations (when the relative error reaches 10^{-5}) of the adaptive procedure employing the APRIORI hp -strategy (*left*) and a zoom in $[-10^{-7}, 10^{-7}] \times [-10^{-7}, 10^{-7}]$ near the re-entrant corner (*right*).

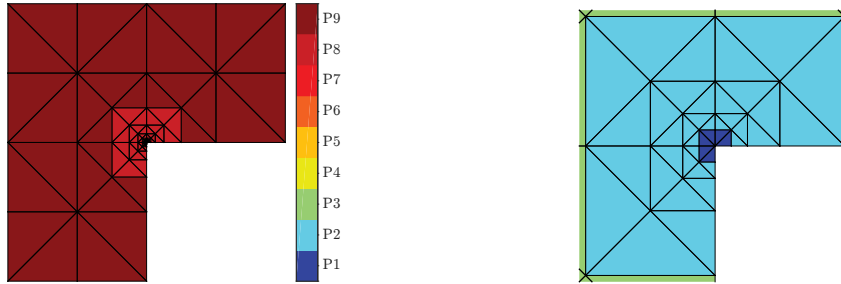


Figure 12: [L-shape domain of Section 6.2] Mesh and polynomial-degree distribution obtained after 45 iterations (when the relative error reaches 10^{-5}) of the procedure employing the refinement strategy LINEAR (*left*) and a zoom in $[-10^{-6}, 10^{-6}] \times [-10^{-6}, 10^{-6}]$ near the re-entrant corner (*right*).

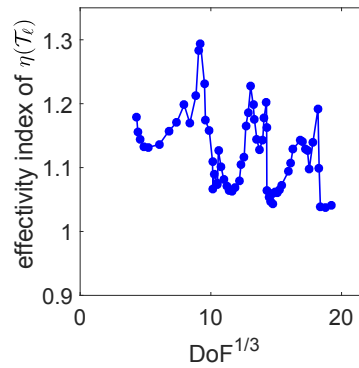


Figure 13: [L-shape domain of Section 6.2] The effectivity indices of the error estimate $\eta(\mathcal{T}_\ell)$, defined as $\eta(\mathcal{T}_\ell)/\|\nabla(u - u_\ell)\|$, throughout the 65 iterations of the present hp -adaptive procedure.

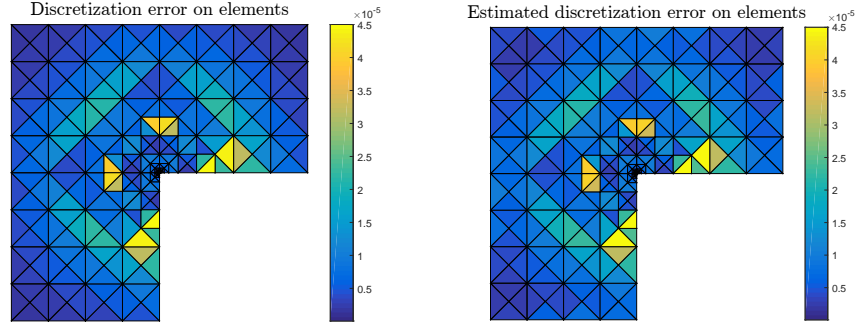


Figure 14: [L-shape domain of Section 6.2] Distribution of the energy error $\|\nabla(u - u_\ell)\|_K$ (left) and of the local error estimators η_K from Theorem 3.2 (right), $\ell = 45$. The effectivity index of the estimate defined as $\eta(\mathcal{T}_{45})/\|\nabla(u - u_{45})\|$ is 1.0468.

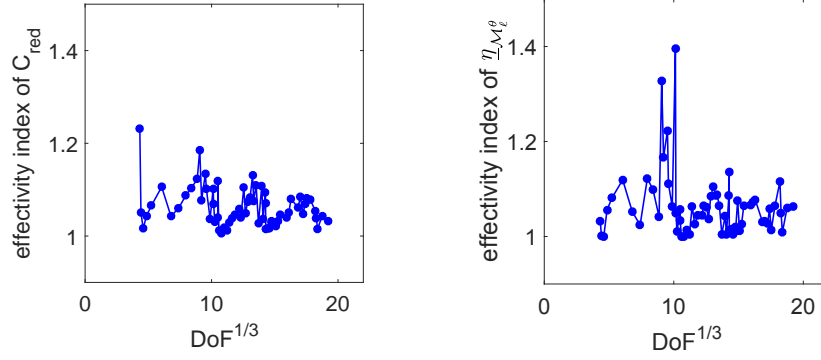


Figure 15: [L-shape domain of Section 6.2] Effectivity indices (6.2) for the error reduction factor C_{red} from Theorem 5.2 (left) and effectivity indices for the lower bound $\underline{\eta}_{\mathcal{M}_\ell^\theta}$ from Lemma 5.1 defined as the ratio $\|\nabla(u_{\ell+1} - u_\ell)\|_{\omega_\ell} / \underline{\eta}_{\mathcal{M}_\ell^\theta}$ (right).

Iteration	1	2	3	4	5	6	7	8	9	10
Triangles	192	192	192	192	192	198	204	210	216	222
Maximal polynomial degree	1	2	3	4	5	5	5	5	5	5
Marked vertices	1	1	1	2	2	3	4	4	6	6
Triangles flagged for h -refinement	0	0	0	0	6	6	6	6	6	6
Triangles flagged for p -refinement	6	6	6	12	6	12	16	18	16	18
Triangles flagged for hp -refinement	0	0	0	0	2	0	0	0	0	0

Table 3: [L-shape domain of Section 6.2] Refinement decisions in Algorithm 2 during the first 10 iterations of the adaptive loop (1.2).

Iteration	56	57	58	59	60	61	62	63	64	65
Triangles	492	512	518	524	538	568	574	580	614	660
Maximal polynomial degree	5	5	5	5	5	5	5	5	5	5
Marked vertices	4	4	5	4	3	3	3	4	5	5
Triangles flagged for h -refinement	16	6	6	6	18	6	6	28	30	32
Triangles flagged for p -refinement	8	16	13	22	0	6	6	0	0	8
Triangles flagged for hp -refinement	0	0	0	0	0	0	0	0	0	4

Table 4: [L-shape domain of Section 6.2] Refinement decisions in Algorithm 2 during the last 10 iterations of the adaptive loop (1.2).

		our	APRIORI	PRIOR	PARAM 0.3	PARAM 0.6
Sharp Gaussian	iter	27	–	37	36	40
(relative error 10^{-3})	DoF $^{1/3}$	12.56	–	14.29	14.06	12.49
L-shape domain	iter	65	70	68	67	68
(relative error 10^{-5})	DoF $^{1/3}$	19.24	17.35	20.82	20.07	18.18

Table 5: Comparison of the different adaptive hp -strategies in terms of the number of iterations of the loop (1.2) and of the number of degrees of freedom necessary to reach the given relative error for model problems of Sections 6.1 and 6.2.

7. Conclusions

In this work, we have devised an hp -adaptive strategy to approximate model elliptic problems using conforming finite elements. Mesh vertices are marked using polynomial-degree-robust a posteriori error estimates based on equilibrated fluxes. Then marked vertices are flagged either for h - or for p -refinement based on the solution of two local finite element problems where local residual liftings are computed. Moreover, by solving a third local finite element problem once the hp -decision has been taken and the next mesh and polynomial-degree distribution have been determined, it is possible to compute a guaranteed bound on the error reduction factor. Our numerical experiments featuring two-dimensional smooth and singular weak solutions indicate that the present hp -adaptive strategy leads to asymptotic exponential convergence rates with respect to the total number of degrees of freedom employed to compute the discrete solution. Moreover, our bound on the error reduction factor appears to be, in most cases, quite sharp. Several extensions of the present work can be considered. On the theoretical side, it is important to prove that our bound on the reduction factor C_{red} is smaller than one and to study how it depends on the mesh-size and especially on the polynomial degree. On the numerical side, three-dimensional test cases and taking into account an inexact algebraic solver are on the agenda.

References

- [1] I. BABUŠKA AND B. GUO, *The h - p version of finite element method, part 1: The basic approximation results*, *Comp. Mech.*, (1986), pp. 21–41.
- [2] ———, *The h - p version of finite element method, part 2: General results and application*, *Comp. Mech.*, (1986), pp. 203–220.
- [3] R. E. BANK, A. PARSANIA, AND S. SAUTER, *Saturation estimates for hp -finite element methods*, *Comput. Vis. Sci.*, 16 (2013), pp. 195–217.
- [4] P. BINEV, *Instance optimality for hp -type approximation*, *Oberwolfach Reports*, 39 (2013), pp. 14–16.

- 380 [5] ———, *Tree approximation for hp-adaptivity*, IMI Preprint Series, 7 (2015).
- [6] D. BRAESS, V. PILLWEIN, AND J. SCHÖBERL, *Equilibrated residual error estimates are p-robust*, *Comput. Methods Appl. Mech. Engrg.*, 198 (2009), pp. 1189–1197.
- [7] M. BÜRG AND W. DÖRFLER, *Convergence of an adaptive hp finite element strategy in higher space-dimensions*, *Appl. Numer. Math.*, 61 (2011),
385 pp. 1132–1146.
- [8] C. CANUTO, R. H. NOCHETTO, R. STEVENSON, AND M. VERANI, *Convergence and optimality of hp-AFEM*, *Numer. Math.*, (2016), pp. 1–47.
- [9] ———, *On p-robust saturation for hp-AFEM*, *Comput. Math. Appl.*, 73
390 (2017), pp. 2004–2022.
- [10] C. CARSTENSEN, M. FEISCHL, M. PAGE, AND D. PRAETORIUS, *Axioms of adaptivity*, *Comput. Math. Appl.*, 67 (2014), pp. 1195–1253.
- [11] J. M. CASCÓN, C. KREUZER, R. H. NOCHETTO, AND K. G. SIEBERT, *Quasi-optimal convergence rate for an adaptive finite element method*,
395 *SIAM J. Numer. Anal.*, 46 (2008), pp. 2524–2550.
- [12] J. M. CASCÓN AND R. H. NOCHETTO, *Quasioptimal cardinality of AFEM driven by nonresidual estimators*, *IMA J. Numer. Anal.*, 32 (2012), pp. 1–29.
- [13] L. DEMKOWICZ, W. RACHOWICZ, AND P. DEVLOO, *A fully automatic hp-adaptivity*, in *Proceedings of the Fifth International Conference on Spectral and High Order Methods (ICOSAHOM-01) (Uppsala)*, vol. 17, 2002,
400 pp. 117–142.
- [14] P. DESTUYNDER AND B. MÉTIVET, *Explicit error bounds in a conforming finite element method*, *Math. Comp.*, 68 (1999), pp. 1379–1396.

- 405 [15] V. DOLEJŠÍ, A. ERN, AND M. VOHRALÍK, *hp-adaptation driven by polynomial-degree-robust a posteriori error estimates for elliptic problems*, SIAM J. Sci. Comput., 38 (2016), pp. A3220–A3246.
- [16] W. DÖRFLER, *A convergent adaptive algorithm for Poisson’s equation*, SIAM J. Numer. Anal., 33 (1996), pp. 1106–1124.
- 410 [17] W. DÖRFLER AND V. HEUVELINE, *Convergence of an adaptive hp finite element strategy in one space dimension*, Appl. Numer. Math., 57 (2007), pp. 1108–1124.
- [18] T. EIBNER AND J. M. MELENK, *An adaptive strategy for hp-FEM based on testing for analyticity*, Comput. Mech., 39 (2007), pp. 575–595.
- 415 [19] A. ERN AND M. VOHRALÍK, *Polynomial-degree-robust a posteriori estimates in a unified setting for conforming, nonconforming, discontinuous Galerkin, and mixed discretizations*, SIAM J. Numer. Anal., 53 (2015), pp. 1058–1081.
- [20] ———, *Stable broken H^1 and $\mathbf{H}(\text{div})$ polynomial extensions for polynomial-degree-robust potential and flux reconstruction in three space dimensions*. HAL Preprint 01422204, submitted for publication, 2016.
- 420 [21] W. GUI AND I. BABUŠKA, *The h, p and h-p versions of the finite element method in 1 dimension. II. The error analysis of the h- and h-p versions*, Numer. Math., 49 (1986), pp. 613–657.
- 425 [22] ———, *The h, p and h-p versions of the finite element method in 1 dimension. III. The adaptive h-p version*, Numer. Math., 49 (1986), pp. 659–683.
- [23] P. HOUSTON AND E. SÜLI, *A note on the design of hp-adaptive finite element methods for elliptic partial differential equations*, Comput. Methods Appl. Mech. Engrg., 194 (2005), pp. 229–243.
- 430 [24] C. KREUZER AND K. G. SIEBERT, *Decay rates of adaptive finite elements with Dörfler marking*, Numer. Math., 117 (2011), pp. 679–716.

- [25] W. F. MITCHELL AND M. A. MCCLAIN, *A comparison of hp-adaptive strategies for elliptic partial differential equations (long version)*, NISTIR 7824, National Institute of Standards and Technology.
- 435 [26] ———, *A comparison of hp-adaptive strategies for elliptic partial differential equations*, ACM Trans. Math. Software, 41 (2014), pp. Art. 2, 39.
- [27] P. MORIN, R. H. NOCHETTO, AND K. G. SIEBERT, *Convergence of adaptive finite element methods*, SIAM Rev., 44 (2002), pp. 631–658 (2003). Revised reprint of “Data oscillation and convergence of adaptive FEM” [SIAM
- 440 J. Numer. Anal. 38 (2000), no. 2, 466–488; MR1770058 (2001g:65157)].
- [28] ———, *Local problems on stars: a posteriori error estimators, convergence, and performance*, Math. Comp., 72 (2003), pp. 1067–1097.
- [29] R. H. NOCHETTO, K. G. SIEBERT, AND A. VEESER, *Theory of adaptive finite element methods: an introduction*, in Multiscale, nonlinear and
- 445 adaptive approximation, Springer, Berlin, 2009, pp. 409–542.
- [30] E. G. SEWELL, *Automatic generation of triangulations for piecewise polynomial approximation*, ProQuest LLC, Ann Arbor, MI, 1972. Thesis (Ph.D.)—Purdue University.
- [31] R. STEVENSON, *Optimality of a standard adaptive finite element method*,
- 450 Found. Comput. Math., 7 (2007), pp. 245–269.
- [32] E. SÜLI, P. HOUSTON, AND C. SCHWAB, *hp-finite element methods for hyperbolic problems*, in The mathematics of finite elements and applications, X, MAFELAP 1999 (Uxbridge), Elsevier, Oxford, 2000, pp. 143–162.
- [33] B. SZABÓ AND I. BABUŠKA, *Finite element analysis*, A Wiley-Interscience
- 455 Publication, John Wiley & Sons Inc., New York, 1991.